

Study of Spatial Resolution of Muon Hodoscopes for Muography Applications in Geophysics

R. Calderón-Ardila^{a,c,d,*}, A. Almela^{a,e}, M. Gómez-Berisso^{c,f}, A. Sedoski^a, C. Varela^a, A. Vesga-Ramírez^{b,c}, H. Asorey^{a,c,f}

^a*Instituto de Tecnologías en Detección y Astropartículas, 1650, Centro Atómico Constituyentes, Buenos Aires, Argentina.*

^b*International Center of Earth Sciences, Comisión Nacional de Energía Atómica, Buenos Aires, Argentina.*

^c*Consejo Nacional de Investigaciones Científicas y Técnicas, CONICET, Argentina.*

^d*Instituto Sabato, Universidad Nacional de San Martín, Centro Atómico Constituyentes, Buenos Aires, Argentina*

^e*Universidad Tecnológica Nacional, Facultad Regional Buenos Aires, Argentina*

^f*Centro Atómico Bariloche and Instituto Balseiro, Comisión Nacional de Energía Atómica and Universidad Nacional de Cuyo, San Carlos de Bariloche, Argentina*

Abstract

Muon radiography, also known as muography, is a non-destructive geophysical technique for the study of the internal structure of large objects such as volcanoes. This is possible by constructing an image based on the differential absorption of the directional flux of high-energy atmospheric muons produced during the interaction of cosmic rays with the atmosphere. So this no other source of radiation is required for this technique. Many muon telescopes are being built with crossed scintillator bars and so, the resolution of each panel is essentially given by the total surface of the bar crossings. Enhancing the resolution may require covering the same area with smaller scintillator bars, which adds costs and build complexity as more scintillators and fibers are required. More channels also require more acquisition electronics which have to be synchronized, increasing the complexity of the system, with associated operating issues, and the final cost. In this work, we propose a novel analysis approach to obtain reliable sub-pixel resolution, by measuring and comparing the average signals measured at each end of the scintillation bar. This analysis approach achieves sub-pixel resolutions, augmenting the spatial resolutions of existing designs. To study the feasibility of this technique we designed a laboratory setup, to emulate muon light pulses with a pulsed laser light located at different points

*Corresponding author

Email address: rolando.calderon@iteda.cnea.gov.ar (R. Calderón-Ardila)

on optical wavelength shifter fiber. By doing this we measured an increase on the spatial resolution when compared with traditional systems. These results enable the design of a new prototype for muography of natural and artificial structures of strategic interest.

Keywords: Muography, Muon Imaging, Volcanoes, Cosmic Ray Techniques, Experimental Particle Physics.

2010 MSC: 00-01, 35Q86, 86-05

1. Introduction

To study volcanic structures using the muography technique [1, 2] an instrument is required that can detect muons. So that, for given exposure time, an image of the dome or volcanic structure can be constructed in terms of density contrast. Conceptually it is similar to an X-ray, but with atmospheric muons as the radiation source [3]. The accuracy of the obtained image depends mainly on the spatial resolution of the instrument and the exposure time. In Latin America detectors have been developed for this purpose, such as the study of the internal structure of the Pyramid of the Sun in Mexico [4] and the MuTe project in Colombia [5, 6]. Some designs are made up of arrays of plastic scintillators, a material capable of producing luminescence when a charged particle passes through them. For most plastic scintillator designs, the spatial resolution depends on the total area where scintillators cross each other.

Recent research in muograph construction mentioned above motivate this work to study a possible improvement of the spatial resolution in plastic-scintillator based muographs [7]. This research is the result from a technology transference from the experience gained from the AMIGA project [8] at the Pierre Auger Observatory in Argentina, which developed and built detectors capable of counting atmospheric muons to study the muonic component of cosmic ray showers.

2. The Muon Radiography

Volcano muography is a technique that uses the directional flux of atmospheric muons to obtain a mass density image of a volcanic structure [9]. Figure 1 shows an illustrative image of a muograph setup for measuring a volcanic dome and the resulting image [6], in this case, the Machin volcano in Colombia [10, 11]. The flux of muons has a dependence on the zenith angle and the mass traversed by the impinging muons.

By knowing the flux and morphology of the geological target it is possible to produce an image from the correlation between the muon count in each direction made with a muon telescope and the distances crossed inside the object [12, 13]. In this way, it is possible to calculate the average opacity along the

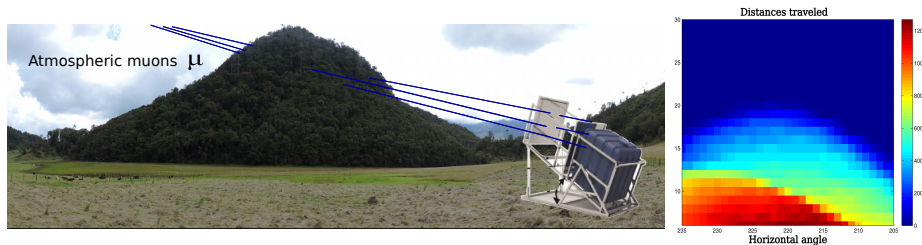


Figure 1: Representation of Muon telescope project (MuTe) in Colombia where scintillator bars of rectangular cross section are used (left). A reconstruction of the mass traversed by the muon flux is shown to the right. For these detectors the resolution depends on the grid formed by the amount of scintillator bars.

muon trajectories in the material traversed and to determine the density contrast in the final image. Additionally, these calculations can be compared with simulations and synthetic data obtained by modeling the target [14, 15] and the muon flux [16, 17].

The muography technique has been used on some volcanoes around the world, such as Mt. Vesuvius by the Mu-RAY project [18]. This project built a muon telescope using three panels consisting of plastic scintillators with a triangular cross-section, coupled to optical fibers with silicon photomultipliers. It has also been used in Japan where it has been successfully deployed on volcanoes such as Mt. Satsuma-Iwojima [9], Mt. Sukuba [19] and Mt. Asama [20], studied using photographic emulsion.

In Italy, muography has been used as a complementary technique to study Mt. Etna [21], but the morphology of the volcano hampered the data analysis; the authors reported differences between synthetic models and measured data. These differences are explained by muon attenuation and electronic noise from the detector. In Colombia, the MuTe telescope [22, 5, 23] uses rectangular cross-section bars made of organic scintillator, wavelength shift optical fibers, photomultipliers, and acquisition electronics. It is a hodoscope composed of arrays of scintillator bars called panels, each consisting of $N_i \times N_j$ bars. These panels are attached to a mechanical structure, setting up the hodoscope.

In this case the resolution of the panels is determined by the number of crosses of the bars or pixels of the hodoscope. To obtain a muography image, it is required to know a priori the properties of the object of study, for example in the case of a volcanic dome it is required to know its morphology and composition, with this information to build a model of the object of study. Then make the acquisition of directional flux of muons with the instrument, Then determine the trajectories of the muons, estimate the attenuation of the flux in terms of opacity and finally make a geophysical inversion between the model and the data obtained, like [24, 25, 26] to obtain the average density for each pixel as a function of the number of muons detected.

This work focuses on studying the improvement of the spatial resolution of

this type of panels by performing a double detection for each scintillator bar, to determine the position of the bar where muons crossed, signal strength is measured at each end of the scintillator fiber. The methodology proposed in this work will be applied to a muograph prototype to be developed and built at Instituto de Tecnologías en Detección y Astropartículas (ITeDA)¹. One of the candidates for field acquisition is the lago Las Mellizas, located on the Copahue Volcano system in Argentina. This lagoon is supported on a natural dam, and presents an opportunity to use the technique to seek changes due to seismic movements or the undermining of the reservoir.

3. Instrumentation

The prototype muograph that motivated this work will be composed of plastic scintillator bars doped with 1 % of PPO [2,5-diphenyloxazole] and 0.03 of the POPOP [1,4-bis(5-phenyloxazole-2-yl)benzene], with a TiO₂ coating [27], coupled at one side to an optical wavelength-shifter fiber. These fibers are the multi-layer reference BCF99-29AMC manufactured by Saint-Gobain, have a diameter of 1.2 mm and produce a wavelength shift of the photons produced in the scintillator.

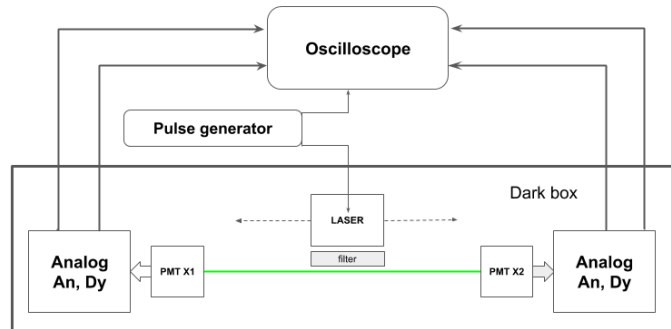


Figure 2: Diagram representing the setup designed and built to determine the position of an event from the signal detected synchronously with two acquisition electronics and a pulse generator. Inside the dark box, the position of the laser represents the location of the artificially generated event.

When a muon passes through the scintillator, a portion of the photons produced are adsorbed and re-emitted by the wavelength shifter (WLS) fibers to finally

¹Instituto ITeDA <http://www.iteda.cnea.gov.ar/>

be guided to one channel of a H8804-b 64-anode photomultiplier manufactured by Hamamatsu. The pulses generated at the PMT are saved, analyzed and identified as events. This detection sequence has been tested and is used by the AMIGA project [8] and the MuTe project [11, 28].

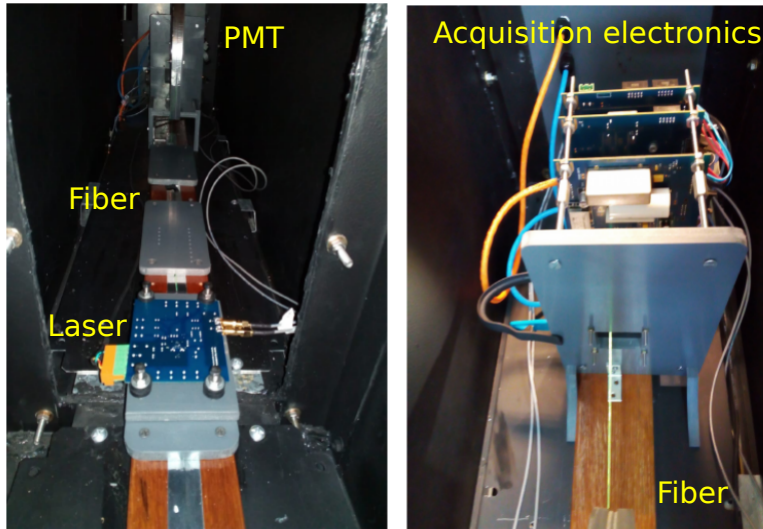


Figure 3: Dark box and setup built to perform the synchronous detection. The dark box was designed and built as a light insulator. Inside the dark box a WLS fiber was installed, with a device designed to install a pulsed laser light source at different positions (left). Each end of the WLS fiber is coupled to a PMT channel and acquisition electronics (right).

The charge of a PMT pulse is given mainly by the amount of photons sensed. The light arriving to one end of the fiber depends on the light adsorbed by the fiber and the light attenuation, which is a function of the distance from the measurement point to the point of adsorption. We characterized these effects with an experimental setup consisting of a WLS fiber coupled at each end to a PMT channel and its associated acquisition electronics. This setup allows the placement of a light source at different positions.

We chose a 405 nm laser to act as a light source, which has a similar wavelength to the light emitted by the plastic scintillator. This laser is triggered by a pulsed laser driver, driven by a pulse generator (Agilent N8042A) that can generate pulses with a similar duration to a typical muon pulse and provides synchronization to the acquisition electronics. A diagram of this setup is shown in figure 2. Fifty thousand samples were acquired for each position using an oscilloscope (LeCroy WaveSurfer 104MXs-B).

As described in section 4 The PMTs used for this characterization is calibrated, to obtain the expected charge for each photo-electron [29]. After both PMTs were calibrated, measurements were taken at 24 separate positions on a 180 cm long fiber every 5 cm. The schematic drawing of the setup is presented in figure

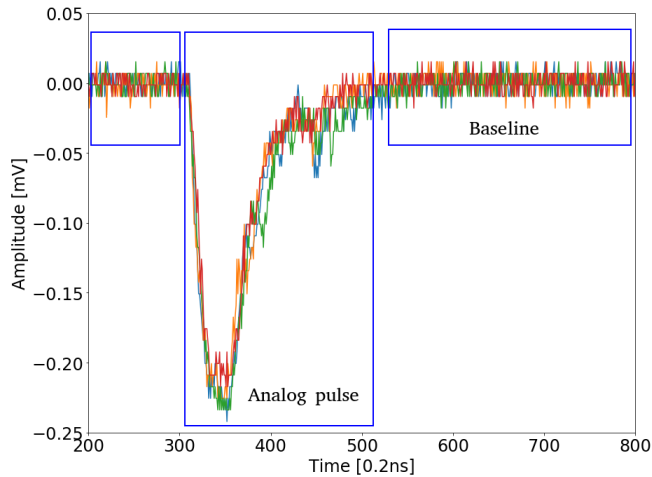


Figure 4: Typical AMIGA PMT pulses from a single anode, measured with a $50\ \Omega$ impedance. Each PMT has 64 outputs (“channels”) corresponding to the anodes. Each channel produces analog pulses as shown in this figure. For each anode, the pulse amplitude is always proportional to the number of impinging photons on the photocathode. For the dynode, the pulse amplitude is proportional to the response from all anodes to the impinging photons.

2. For each position, the histograms of the deposited charge at each end were obtained. The charge was calculated from the oscilloscope traces by subtracting the baseline from the pulse and applying a point-to-point integration in a fixed time window corresponding to the area defined as the analog pulse (see figure 4), so that each point will have a charge value $Q_t = \sum_a^b A(t)dt$.

Then, based on these histograms, the number of photo-electrons detected was calculated as a function of the distance. This function is the crucial part of the methodology: on a muograph, it provides an accurate estimation of the impact point of the particle within the scintillator strip, enhancing the resolution of the device.

4. Data acquisition

The PMT used allows the acquisition of its 64 independent anodes and a common dynode, which integrates the charge collected by the anodes. For calibration and measurement it was necessary to condition the light source by using Kodak optical filters. For the PMT calibration, this was done to ensure a photon count at the PMT photocathode of less than one photon per event due to quantum efficiency effects. For data acquisition, this was done to simulate different muonic responses.

To calculate the mean of photon-electrons we fitted the acquired data with a PMT response model adapted from [29]. With this model we obtained the best

fit for low light emission conditions where most detected events correspond to a single photon.

The model used for the PMT response was augmented to obtain the charge ratio between an anode and the dynode. This ratio is critical to the proposed mugraph prototype, as the AMIGA electronics does not allow the charge measurement of the anode. As we are planning to operate the detector by measuring the charge at the dynode, we discarded events where more than one anode detects signal. Given the expected muon flux for muography applications, this does not result in a significant event discard rate, and therefore does not increase the required exposure time.

4.1. PMT Calibration

The calibration method is based on the deconvolution of the pulse spectrum into a noise component and a pulse component, discriminated by number of photoelectrons sensed. The characteristic parameters each number of photoelectrons detected are then also expressed as a function of the parameters for a single detected photoelectron.

An ideal PMT can be treated as an instrument consisting of two independent parts: a photodetector, where a photon flow is converted into photoelectrons, and an amplifier based on a dynode chain, which amplifies the initial charge emitted by the photocathode.

The flux of photons impinging on the PMT photocathode produces photoelectrons through the photoelectric effect. For the photo conversion the Q_E -quantum efficiency is evaluated and described by:

$$\mu = \mu_\rho Q_E \quad (1)$$

where μ is the average number of photoelectrons emitted and μ_ρ the average number of incident photons. The number of photoelectrons emitted by the photocathode is a Poisson process, where μ is the average number of photoelectrons collected by the first dynode. This model yields the equation:

$$P(n; \mu) = \frac{\mu^n e^{-\mu}}{n!} \quad (2)$$

where $P(n; \mu)$ is the probability of observing n photo-electrons when the average amount of photoelectrons detected per event is μ . Furthermore, when an average number of μ_ρ photons imping on the photocathode per event, the quantum efficiency of the photocathode is Q_E . Thus, for a given PMT, the parameter μ characterizes the intensity of the light source, taking into account the quantum efficiency of the photocathode and the efficiency of the electron collection of the dynode system.

For the amplification response we model the dynode chain, where in each stage of the amplification cascade we have a Gaussian distribution [30]. The total response of the amplification chain is the sum of the response of each dynode, giving the equation:

$$G(x) = \frac{1}{\sigma\sqrt{2\pi}} e^{-\frac{(x-q)^2}{2\sigma^2}} \quad (3)$$

where x is the charge received at the first dynode, q is the average charge at the PMT output when an electron is picked up by the first dynode (single photo-electron, SPE) and σ is the standard deviation of the entire amplification chain.

The charge distribution of a process initiated by n photo-electrons is the convolution of n processes with an SPE, therefore we can approximate the ideal response of the PMT without the noise as the convolution of the distributions 2 and 3:

$$S_{ideal}(x) = P(n_{SP}; u) \otimes G_n(x) \quad (4)$$

obtaining an ideal charge model for the PMT:

$$S_{ideal}(x) = \sum_{n=0}^{\infty} \frac{u^n \cdot e^{-u}}{n!} \cdot \frac{1}{\sigma\sqrt{2\pi}} \cdot e^{-\frac{(x-n \cdot q)^2}{2n\sigma^2}} \quad (5)$$

This distribution alone does not represent the response of a real PMT due to device noise. Background noise processes (such as *dark current*, *afterpulse* and *cross-talk*) can generate additional current signals that modify the output response.

These background processes can be divided into two groups, with different distribution functions: low charge processes and discrete processes. Low-charge processes are responsible for non-zero current when there are not photo-electrons emitted from the photocathode. This distribution corresponds to the pedestal and can be modelled with a Gaussian function.

$$N_G(x) = \frac{1}{\sigma_o\sqrt{2\pi}} e^{-\frac{(x-q_o)^2}{2\sigma_o^2}} \quad (6)$$

The discrete processes can be thermo-emission (electrons detached from the photocathode without an impinging photon) and noise initiated by the measured light with probability other than zero. These processes accompany the measured signal and can be modeled with an exponential distribution.

$$N_E(x) = \lambda e^{x\lambda} \quad (7)$$

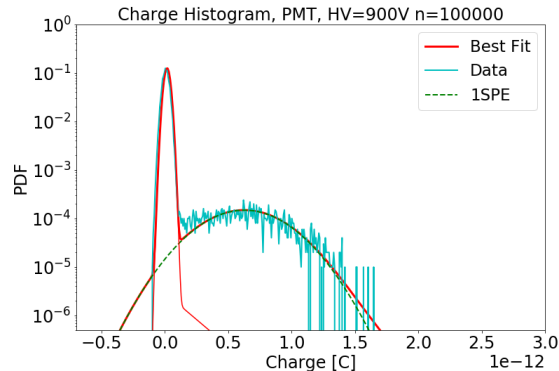


Figure 5: Calibration histogram for a PMT. 100.000 samples were taken in low light conditions for this purpose. The image contains two peaks: the first (leftmost) peak represents the most likely charge value for background noise, while the second (rightmost) peak represents the average charge for an SPE.

If call w to the probability that a measured signal is accompanied by a background process, the background noise processes can be parameterized as:

$$N(x) = \frac{(1-w)}{\sigma_o \sqrt{2\pi}} e^{-\frac{(x-q_o)^2}{2\sigma_o^2}} + w\lambda e^{x\lambda} \quad (8)$$

The first term corresponds to the discrete processes. The second term corresponds to low charge background processes (pedestal). For small $\sigma_o (\ll 1/\lambda)$ (good baseline), the convolution of a Gaussian with an exponential function is reduced to a pure exponential function.

Using the spectrum for an ideal PMT from equation 5 and the background charge distribution in equation 8, the response spectrum for a realistic PMT can be obtained as the convolution of both distributions:

$$S_{real}(x) = S_{ideal}(x) \otimes N(x) \quad (9)$$

The response function for a real PMT contains seven free parameters and was developed at [31]. Two of them, q_o and σ_o , define the pedestal and two others, w and λ , describe the discrete background processes. Finally the parameters q , σ and μ describe the spectrum of the real signal. Of these three parameters, μ is proportional to the intensity of the light source, and q and σ characterize the amplification process of the PMT dynode system. Finally, we use the $S_{real}(x)$ response model to compare and calibrate the response of the PMTs.

4.2. Measurements using expected operation conditions

After the PMTs were calibrated, we removed some of the light filters from the setup to simulate operating conditions and proceeded to measure pulses, moving

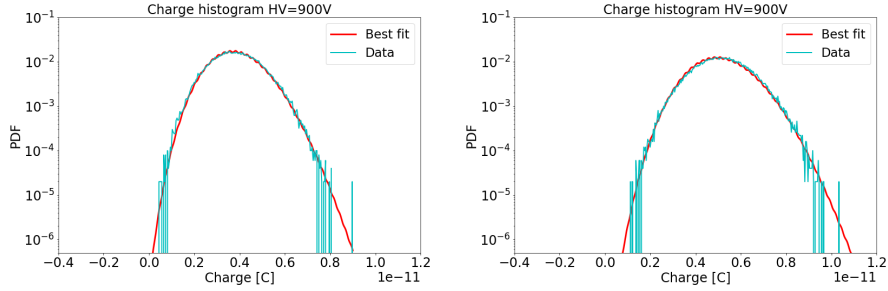


Figure 6: Histogram for an acquisition with an average of 14 SPEs (left), and 20 SPEs (right). For each histogram, 50.000 acquisitions were considered. In both histograms the pedestal is not visible because at these light intensities and for this PMT most events detect at least one SPE.

the light source as described in 3.

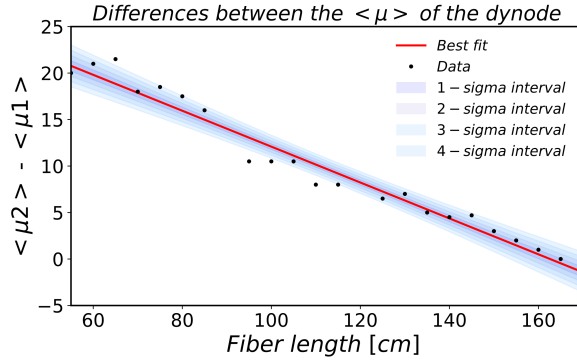


Figure 7: After the calibration, the light source was moved lengthwise along the optical fiber. 50.000 samples were taken at each light source position, and the μ was estimated for both electronics. Then we proceeded to subtract the μ calculated for each PMT at every position, then used these values to estimate the best fit and represent the confidence intervals in function of the σ error. In this picture we compare the measurements with the fit confidence intervals from 1- σ to 4- σ .

Thus we could establish the location within the bar according to the absolute difference in terms of μ . In each case μ was calculated from the fit values of the calibration for each PMT. At each position, 50,000 pulses were acquired, obtaining charge histograms as shown in figure 5.

Then we subtracted the average number of photo-electrons measured at each position and determined the numbers of photoelectrons for each distance to the light source, obtaining the confidence intervals observed in figure 7 and 8.

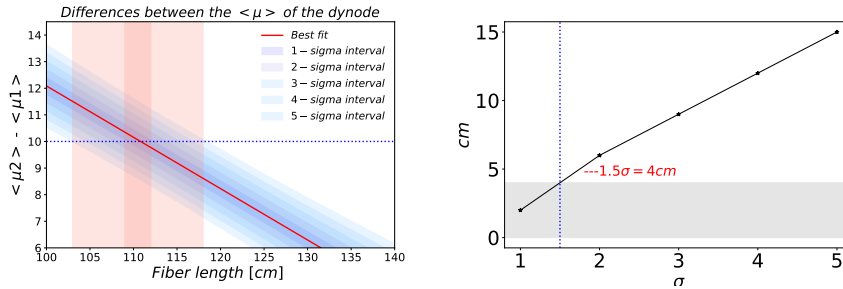


Figure 8: Left: Projection of the confidence intervals as a function of the distance between the photocathode and the light source. Right: Comparison of the uncertainty in terms of sigma σ for different fiber lengths, using data from the previous plot. 1.5σ represents the maximum acceptable uncertainty for a 4 x 4 cm pixel.

5. Conclusions

A methodology and design modification to enhance the spatial resolution of a muograph was proposed. An experimental setup using a movable controlled light source synchronized with acquisition electronics was built to test the feasibility of the proposed methodology. This setup was used to calibrate PMTs using a PMT response model adapted to the proposed analysis methodology.

Using this setup with light intensities similar to expected as operating conditions, we could determine the position of the light source from the charge measured by the dynode of the PMTs at both ends of the fiber. The confidence intervals of the measurements in operating conditions yielded favorable information about the uncertainty when determining the impact position using this strategy. From these results we can estimate 3 cm with a 1σ of error with respect to the fit. Since the muon flux is a known measurement, we can also estimate the exposure time to acquire enough events. Therefore, this methodology is feasible.

Due to the measurement setup, no scintillator effects were considered. The experimental setup can be used to evaluate different optical fibers and light sensing devices. The setup also allows the use of a scintillator strip as a light source, with a muon telescope as described in [32]. A prototype detector will be built to further test this methodology.

6. Acknowledgments

The authors are very thankful to the participating institutions, Instituto de Tecnologías en Detección y Astropartículas (ITeDA), The National Scientific and Technical Research Council (CONICET), The Comisión Nacional de Energía Atómica (CNEA), Universidad Tecnológica Nacional (UTN), Universidad Nacional de Cuyo (UCN) and Pierre Auger Collaboration for their support. In

addition, some results presented in this paper were carried out using the ITeDA computer cluster maintained by CNEA in Argentina.

References

- [1] L. W. Alvarez, J. A. Anderson, F. El Bedwei, J. Burkhard, A. Fakhry, A. Girgis, A. Goneid, F. Hassan, D. Iverson, G. Lynch, et al., Search for hidden chambers in the pyramids, *Science* 167 (3919) (1970) 832–839.
- [2] K. N. Borozdin, G. E. Hogan, C. Morris, W. C. Priedhorsky, A. Saunders, L. J. Schultz, M. E. Teasdale, Radiographic imaging with cosmic-ray muons, *Nature* 422 (6929) (2003) 277–277.
- [3] L. Bonechi, R. DAlessandro, A. Giammanco, Atmospheric muons as an imaging tool, *Reviews in Physics* (2020) 100038.
- [4] A. Menchaca-Rocha, Using cosmic muons to search for cavities in the pyramid of the sun, teotihuacan: preliminary results, *PoS* (2014) 012.
- [5] H. Asorey, A. Balaguera-Rojas, L. A. Núñez, J. D. Sanabria-Gómez, C. Sarmiento-Cano, M. Suárez-Durán, M. Valencia-Otero, A. Vesga-Ramírez, Astroparticle Techniques: Colombia Active Volcano Candidates for Muon Telescope Observation Sites, in: *Revista Mexicana de Astronomía y Astrofísica Conference Series*, Vol. 49, 2017, pp. 54–54. [arXiv: 1704.04967](https://arxiv.org/abs/1704.04967).
- [6] A. Vesga-Ramírez, D. Sierra-Porta, J. Pena-Rodriguez, J. Sanabria-Gomez, M. Valencia-Otero, C. Sarmiento-Cano, M. Suarez-Duran, H. Asorey, L. Nunez, Muon tomography sites for colombian volcanoes, *arXiv* (2017) [arXiv-1705](https://arxiv.org/abs/1705).
- [7] N. Accialini, et al., Amiga status report, Pierre Auger Collaboration internal report (GAP2011 120).
- [8] T. P. A. Collaboration, Prototype muon detectors for the amiga component of the pierre auger observatory, JINST.
URL <http://inspirehep.net/record/1422718?ln=en>
- [9] H. Tanaka, T. Uchida, M. Tanaka, H. Shinohara, H. Taira, Cosmic ray muon imaging of magma in a conduit: Degassing process of satsuma iwajima volcano, japan, *Geophysical Research Letters* 36 (1).
- [10] H. Asorey, R. Caldern-Ardila, K. Forero-Gutiérrez, L. Nuñez, J. Peña-Rodríguez, J. Salamanca-Coy, D. Sanabria-Gómez, J. Sánchez-Villafrades, D. Sierra-Porta, minimute: A muon telescope prototype for studying volcanic structures with cosmic ray flux., *Scientia et Technica* 23 (3) (2018) 386–391.

- [11] J. Peña-Rodríguez, J. Pisco-Guabave, D. Sierra-Porta, M. Suárez-Durán, M. Arenas-Flórez, L. Pérez-Archila, J. Sanabria-Gómez, H. Asorey, L. Núñez, Design and construction of mute: a hybrid muon telescope to study colombian volcanoes, arXiv preprint arXiv:2004.09364.
- [12] D. Varga, G. Hamar, G. Nyitrai, A. Gera, L. Oláh, H. Tanaka, Tracking detector for high performance cosmic muon imaging, *Journal of Instrumentation* 15 (05) (2020) C05007.
- [13] M. Rosas-Carbajal, J. Marteau, M. Tramontini, F. Zyserman, J. Bremond d’Ars, Y. Le Gonidec, B. Carlus, J.-C. Ianigro, S. Deroussi, J.-C. Komorowski, et al., Muon tomography of the la soufrière de guadeloupe hydrothermal system: 3-d structure and dynamics, in: *EGU General Assembly Conference Abstracts*, Vol. 20, 2018, p. 18548.
- [14] C. D. Athanassas, C. Kitsaki, T. Alexopoulos, V. Gika, S. Maltezos, Simulation of a muographic analysis of a volcanic dome in geant4, *HNPS Advances in Nuclear Physics* 27 (2020) 37–47.
- [15] A. Vásquez-Ramírez, M. Suárez-Durán, A. Jaimes-Motta, R. Calderón-Ardila, J. Peña-Rodríguez, J. Sánchez-Villafrades, J. Sanabria-Gómez, H. Asorey, L. Núñez, Simulated response of mute, a hybrid muon telescope, arXiv preprint arXiv:1912.10081.
- [16] C. Sarmiento-cano, M. Suárez-Durán, A. Vásquez-Ramírez, A. Jaimes-Motta, R. Calderón-Ardila, J. Peña-Rodríguez, Modeling the lago’s detectors response to secondary particles at ground level from the antarctic to mexico, *PoS*.
- [17] H. Asorey, L. A. Núñez, M. Suárez-Durán, Preliminary results from the latin american giant observatory space weather simulation chain, *Space Weather* 16 (5) (2018) 461–475.
- [18] G. Ambrosi, F. Ambrosino, R. Battiston, A. Bross, S. Callier, F. Cassese, G. Castellini, R. Ciaranfi, F. Cozzolino, R. DAlessandro, et al., The mu-ray project: Volcano radiography with cosmic-ray muons, *Nuclear Instruments and Methods in Physics Research Section A: Accelerators, Spectrometers, Detectors and Associated Equipment* 628 (1) (2011) 120–123.
- [19] K. Nagamine, M. Iwasaki, K. Shimomura, K. Ishida, Method of probing inner-structure of geophysical substance with the horizontal cosmic-ray muons and possible application to volcanic eruption prediction, *Nuclear Instruments and Methods in Physics Research Section A: Accelerators, Spectrometers, Detectors and Associated Equipment* 356 (2) (1995) 585–595.
- [20] H. Tanaka, T. Nakano, S. Takahashi, J. Yoshida, M. Takeo, J. Oikawa, T. Ohminato, Y. Aoki, E. Koyama, H. Tsuji, et al., Radiographic imaging below a volcanic crater floor with cosmic-ray muons, *American Journal of Science* 308 (7) (2008) 843–850.

- [21] D. Carbone, D. Gibert, J. Marteau, M. Diament, L. Zuccarello, E. Galichet, An experiment of muon radiography at mt etna (italy), *Geophysical Journal International* 196 (2) (2013) 633–643.
- [22] MuTe, Proyecto Muon Telescope, Url <http://halley.uis.edu.co/fuego/>, [Web accessed at 27-04-2020] (2020).
- [23] H. Asorey, A. Balaguera-Rojas, R. Calderón-Ardila, L. A. Núñez, J. D. Sanabria-Gómez, M. Suárez-Durán, A. Tapia, Muon Telescope (MuTe): A first study using Geant4, Vol. 49 of *Revista Mexicana de Astronomía y Astrofísica Conference Series*, 2017, pp. 144–144.
- [24] A. Vesga-Ramírez, J. Sanabria-Gómez, D. Sierra-Porta, L. Arana-Salinas, H. Asorey, V. Kudryavtsev, R. Calderón-Ardila, L. Núñez, Simulated annealing for volcano muography, arXiv preprint arXiv:2005.08295.
- [25] A. Barnoud, V. Cayol, V. Niess, C. Carloganu, P. Lelièvre, P. Labazuy, E. Le Ménèdeu, Bayesian joint muographic and gravimetric inversion applied to volcanoes, *Geophysical Journal International* 218 (3) (2019) 2179–2194.
- [26] C. Benton, C. Mitchell, M. Coleman, S. Paling, D. Lincoln, L. Thompson, S. Clark, J. Gluyas, Optimizing geophysical muon radiography using information theory, *Geophysical Journal International* 220 (2) (2020) 1078–1094.
- [27] A. Pla-Dalmau, A. D. Bross, K. L. Mellott, Low-cost extruded plastic scintillator, *Nuclear Instruments and Methods in Physics Research Section A: Accelerators, Spectrometers, Detectors and Associated Equipment* 466 (3) (2001) 482–491.
- [28] H. Asorey, R. Calderón-Ardila, C. Carvajal-Bohorquez, S. Hernández-Barajas, L. Martínez-Ramírez, A. Jaimes-Motta, F. León-Carreño, J. Peña-Rodríguez, J. Pisco-Guavabe, J. Sanabria-Gómez, et al., Astroparticle projects at the eastern colombia region: facilities and instrumentation, *Scientia et Technica* 23 (3) (2018) 391–396.
- [29] E. Bellamy, G. Bellettini, F. Gervelli, M. Incagli, D. Lucchesi, C. Pagliarone, F. Zetti, Y. Budagov, I. Chirikov-Zorin, S. Tokar, Absolute calibration and monitoring of a spectrometric channel using a photomultiplier, Tech. rep., Joint Inst. for Nuclear Research (1993).
- [30] I. Chirikov-Zorin, I. Fedorko, A. Menzione, I. Sykora, S. Tokar, Precise analysis of the metal package photomultiplier spectra, *Nuclear Instruments and Methods in Physics Research Section A: Accelerators, Spectrometers, Detectors and Associated Equipment* 461 (1-3) (2001) 587–590.
- [31] D. A. Almela, Detectores de muones del observatorio pierre auger: Diseño y técnicas de operación de se electrónica, Ph.D. thesis, Universidad Tecnológica Nacional (2019).

- [32] A. Aab, P. Abreu, M. Aglietta, E. Ahn, I. Al Samarai, I. Albuquerque, I. Allekotte, P. Allison, A. Almela, J. A. Castillo, et al., Prototype muon detectors for the amiga component of the pierre auger observatory, *Journal of Instrumentation* 11 (02) (2016) P02012.